Available online at www.sciencedirect.com

ScienceDirect

Materials Today: Proceedings 5 (2018) 14693–14704

materialstoday: PROCEEDINGS

www.materialstoday.com/proceedings

EDS 2016

# Atomic scale mechanisms and brittle to ductile transition at low size in silicon

Sandrine Brochard[a,*], Firas Abed El Nabi[a], Laurent Pizzagalli[a], Amina Merabet[b], Michaël Texier[b], Christophe Tromas[a], Julien Godet[a]

[a]*Institut Pprime, UPR 3346 CNRS, Université de Poitiers, ISAE-ENSMA, Département Physique et Mécanique des Matériaux, SP2MI – BP 30179, F86962 Futuroscope Chasseneuil Cedex, France*

[b]*IM2NP, UMR 7334 CNRS – Université Aix-Marseille – Université de Toulon,13397 Marseille, France*

**Abstract**

Molecular dynamics (MD) simulations of silicon nanowires (NW) tensile deformation were performed. They reveal a great variety of behaviors, which are rationalized thanks to a diagram highlighting the sequences of elementary mechanisms. In particular, MD simulations show that cavity formation inside the NW can occur through dislocations interactions. To quantify the brittle/ductile character of the NWs for each tested conditions, we define a ductility parameter which is extracted from the simulation output. Its variation suggests that the brittle to ductile transition (BDT) at low size is not sharp, conversely to the well-known BDT for bulk silicon.



Selection and/or Peer-review under responsibility of Extended Defects In Semiconductors 2016 (EDS 2016).

*Keywords:* brittle to ductile transition; silicon; nanowire;molecular dynamics simulations; dislocation; cavity

## 1. Introduction

Mechanical properties of nano-objects or nanostructures are often very different from their bulk counterparts. A typical example is their very high strength [1,2], as for example that of bent silicon nanowires (NWs) [3,4]. Another interesting feature, specific to semiconductors and mainly evidenced through pillars compression experiments, is the brittle to ductile transition (BDT) with the size of the sample at low or room temperature. Indeed, while most

* Corresponding author. Tel.: +33 5 49 49 68 33; fax: +33 5 49 49 66 92.
*E-mail address:* sandrine.brochard@univ-poitiers.fr


Selection and/or Peer-review under responsibility of Extended Defects In Semiconductors 2016 (EDS 2016).

semiconductors are brittle in their bulk form at room temperature, they become ductile below few hundreds of nanometers, as shown for silicon [5,6], as well as for other semiconductors [7-9]. Ductility of silicon NWs at room temperature has also been observed with in situ transmission electron microscopy (TEM) tensile [10] and bending [11,12] experiments.

For bulk silicon, the BDT is associated with the propagation of pre-existing cracks by cleavage at low temperature, whereas crack-tip blunting and dislocation shielding occur at high temperature. The precise temperature of the transition is highly dependent on the experimental conditions (strain rate, doping), but for given conditions the transition is very sharp, happening over a small range of temperature [13-15]. This sharp character has also been evidenced with atomistic simulations [16]. Although it is not necessarily directly related to the BDT, it is worth noting that temperature may also yield a change in plasticity mechanisms, with partial or dissociated dislocations certainly in glide set planes at high temperature and perfect dislocations supposedly in shuffle set planes at low temperature, as shown experimentally in bulk silicon [17] or with molecular dynamics (MD) simulations [18].

For silicon micropillars of fixed size, a BDT with temperature is as well observed, for a temperature lower than in bulk [19,20], and with coexistence of cracks and slip traces at intermediate temperatures [19]. Micropillars compression experiments at high temperature (500°C) have also revealed partial dislocation and twinning mediated plasticity [19]. Note however that there is no available tension experiment at high temperature.

At the microscale and below, experimental studies show that the ductile or brittle character not only depends on the sample size and the temperature, but also on other experimental conditions such as the NW axis [10,21], the deformation mode [11], the surface state [22], not to mention the strain rate. Despite some similarities with bulk BDT (eg the temperature or strain rate dependence), a fundamental change in the nature of the transition at the nanoscale is speculated. Indeed, nano-objects are characterized by a high surface to volume ratio and no pre-existing defects inside the sample, so that the ductile behavior is expected to be governed by dislocation nucleation and propagation from surfaces, which have been proven to be efficient dislocation sources [23-29], whereas the brittle regime would be governed by crack formation.

Atomic simulations are particularly well suited for studying the elementary mechanisms at play, since they allow their direct visualization at the atomic scale and an easy tuning of the test conditions (geometry, temperature,...). Besides, for nano-objects the system sizes considered are in the same range for atomistic simulations and experiments, making the comparison all the more relevant. Like for experiments, atomistic simulation studies exhibit a great variety of mechanical behaviors of Si NW depending on the test conditions [11,30-33]. In order to model systems with sizes comparable to those in experiments, interatomic potentials are used. In contrast to metals, the transferability of the potentials for semiconductors may be limited; the use of different interatomic potentials for the different studies adds then another level of variance in the results [34].

For the present study, we conducted MD simulations with two different interatomic potentials. These are chosen because they fairly reproduce mechanical properties of silicon while having very different forms. Si NWs with a geometry similar to experimental ones were submitted to tensile deformation, which yields to both plasticity and "easy" (as compared to compression) crack formation. The focus of this article is on the one hand on the description of the variety of mechanisms observed at the atomic scale (section 3), and on the other hand on the quantitative assessment of the ductile/brittle character for the different situations encountered in simulations (section 4).

## 2. Model and methods

In this study we have considered cylindrical-shaped silicon NWs with <011> axis (see Fig. 1(a)). Such NWs are close to those commonly considered experimentally [4-6,10,11,19,20,22]; moreover, they have no edges which could concentrate the stress. They were submitted to an axial tensile stress; for the chosen stress orientation, four slip systems with perfect dislocations of Burgers vector ½<110> can be activated with the same maximum Schmid factor (0.41). Thus, this stress orientation favors interactions of dislocations nucleated on the two activated {111} secant planes. Several diameters $d$ and lengths $\ell$ were tested ranging between 8 to 45 nm in diameter, and 8 to 75 nm in length, reaching for some tests a total maximum of 6 million atoms. Periodic boundary conditions were applied along all three space directions. Along the two directions perpendicular to the NW axis, an empty space was

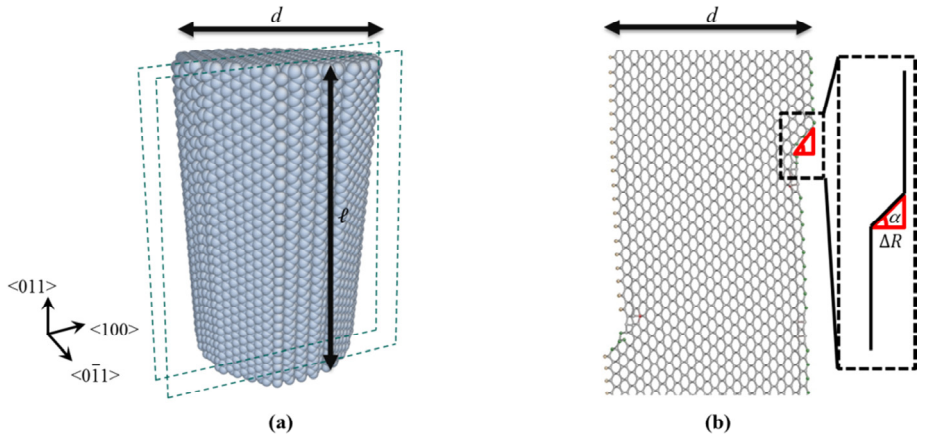


Fig. 1. (a) Geometry of the studied NWs. The dashed lines indicate a typical slice cut in the NW used to visualize the atomic scale mechanisms. (b) Slice cut view with the quantities used for the definition of the ductility parameter (equation (1)).

left, large enough to avoid interactions between the NW and its periodic images. Along the NW axis, the simulation box length was chosen to be equal to the NW length, so as to mimic an infinitely long NW and prevent end effects.

The simulations were performed at low (10K), room (300K) and high (600 and 900K) temperatures. For low temperature deformation tests, two different surface states were considered: (i) fresh-cut surfaces for which nor reconstruction or relaxation is carried out prior to the deformation test, and (ii) annealed surfaces for which a 300 K thermalization is conducted before the NW deformation test. For room and high temperature deformation tests, surfaces were annealed first at 300 K and later at the temperature of the test. Further details about surface states can be found in our previous article [33].

MD simulations were performed with the parallelized open source LAMMPS code [35]. The Verlet algorithm [36] was used to numerically solve the Newton's equation of motion, with a typical time step of 0.5 fs, which is small enough to ensure that there is no energy drift for all the studied temperatures. Temperature was first introduced by giving random initial velocities to all atoms according to the corresponding Maxwell distribution, and maintained using a Nosé-Hoover thermostat [37].

Atomic interactions were modelled with two different potentials. The first one, referred as SW*m*, is a modified version of the well-known Stillinger-Weber potential [38] that offers an improved description of both plasticity and fracture [39], while keeping the superior ability of the original potential to model silicon under high stress [40]. The second one, referred as MEAM-G, is also a new parametrization of an existing form, the modified embedded-atom-method potential proposed by Baskes [41], which has been shown to fairly reproduce fracture properties of silicon NW [34]. For a better account of plasticity properties, we developed our own parametrization, as described in [42] (note that for the present study we set 'delr' parameter to 2.1 Å).

A typical deformation test started with the deformation of the simulation box up to 10%, with a remapping of the atomic positions inside the box, followed by an energy minimization using the conjugate gradient method. This deformation step allowed saving a lot of computation time, while not modifying the further behavior of the system since the applied strain value was below the elasticity limit (estimated through preliminary tests). The NW was then equilibrated in the NVT ensemble for 60 ps at the temperature of the deformation test; for NWs with annealed surfaces, this step can be considered as the second thermalization sequence. Next the NW was deformed during 300 ps at a constant engineering strain rate of $10^8$ $s^{-1}$. This value, typical of MD simulations, is many orders of magnitude higher than the experimental ones. When reducing the strain rate, a reduction of the yield strain is expected [43], which can amount up to 50% when approaching experimental values [44]. Like for the pre-deformation step, strain was there applied by changing the simulation box length and remapping all atoms coordinates to the new box. During the whole run, the system energy was monitored so as to detect the onset of plasticity, characterized by a significant drop of the energy.

To visualize plasticity events, we use both full and slice views of the NW (see Fig. 1), with sometimes the help of the coordination number to highlight only those atoms which are not in a perfect environment. All the figures presented in this article were done with the AtomeEye code [45].

## 3. Atomic scale mechanisms

### *3.1. Elementary mechanisms decomposition*

The analysis of the various MD deformation tests reveals a great variety of behaviors. Even for tests performed under the same conditions, different behaviors can be observed for different initial distributions of atomic velocities. From all the results, we identified a limited number of elementary mechanisms occurring at the atomic scale: dislocation nucleation at the surface or inside the NW, dislocation propagation, dislocation interactions, cavity opening, amorphization and crack tip propagation (or cavity extension). Structural defects – dislocations, cavity and disorder – are produced, grow or interact through these elementary mechanisms. Note that for the range of temperature studied, up to 900K, only perfect dislocations were nucleated and propagated in shuffle set planes.

In order to explain the NW behavior, we use diagrams (Fig. 2) in which the elementary mechanisms, indicated by arrows, connect the structural defects. The whole deformation of the NW can be described by a simple path in this diagram, leading either to ductility (Fig. 2(a)) or to brittleness (Fig. 2(b)); that is for example the case for some of the tests presented in our previous paper [32], with a purely ductile behavior shown in figure 3 therein, and a purely brittle behavior shown in figure 8. Note that these two behaviors were obtained for the same set of parameters (SW*m* potential, fresh-cut surface, 300 K, $d = 8$ nm), except the NW length which was 21 nm for the brittle NW and 8 nm for the ductile one. One important result of the simulations, indicated in [32] and displayed in Fig. 2, is that NW irreversible deformation always starts with dislocation nucleation.

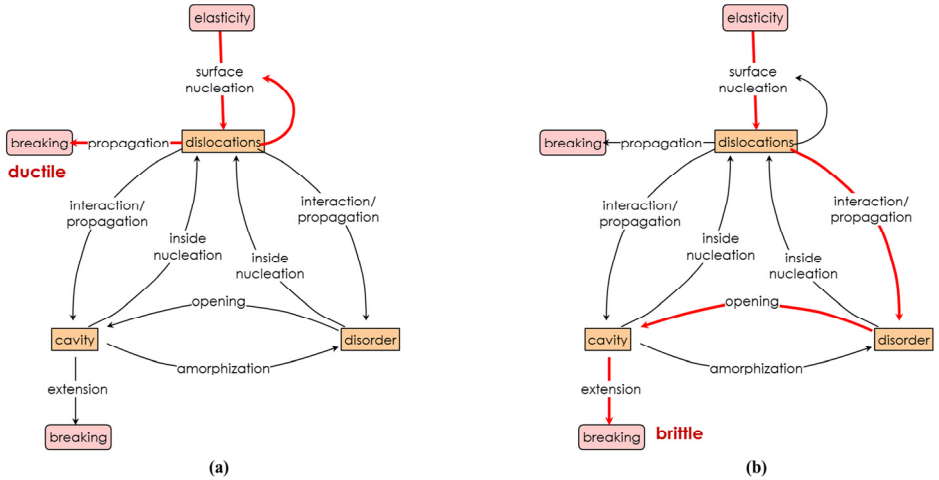


Fig. 2. Elementary mechanisms (arrows) diagram. Structural defects are indicated in orange. (a) Ductile behavior. (b) Brittle behavior.

However, in most simulations, the sequence of elementary mechanisms is not so simple: some parts of the path can be covered several times (loops in the diagram), and / or different mechanisms can occur concurrently, leading to a complex entanglement. In the next section, we present some of the encountered complex sequences.

### *3.2. Complex mechanisms sequences*

Fig. 3 shows the onset of plasticity for one of the biggest NW considered ($d = 45$ nm, $\ell = 46$ nm), and Fig. 4 is the corresponding slice view. The deformation test was performed with SW*m* potential at 10 K, and the NW had a fresh-cut surface. For this run, the first dislocation is nucleated from the NW surface for 17% strain (black arrow in Fig. 3(a)) and glide in a {111} shuffle set plane (red line in Fig. 4(a)). During the propagation of this first dislocation (core circled in red in Fig. 4(b)), the increase of the surface step (black arrows in Fig 4(a) and (b)) suggests that

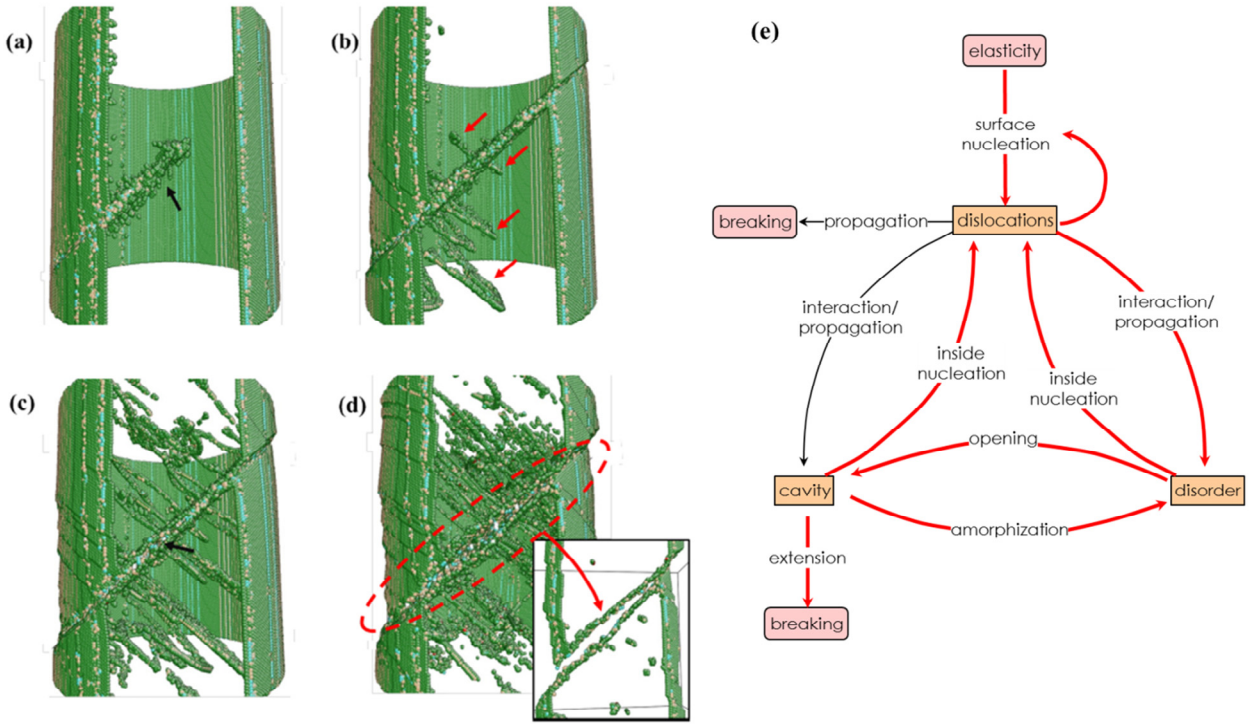


Fig. 3. (a)-(d) Onset of plasticity and crack formation in a 45 nm diameter NW deformed up to 17% in tension at 10 K (SW*m* potential, $\ell$ = 46 nm, fresh-cut surface). Atoms are colored according to their coordination number: green: 3, beige: 2, blue: 1. Atoms in a perfect diamond cubic environment are not shown. See text for details. (e) Corresponding elementary mechanisms (red arrows).

other dislocations are nucleated and glide in the same plane following the first nucleation event. Interestingly, some defects (structural disorder) are formed in the wake of the first nucleated dislocation. The interaction of the following dislocations with these defects increases the disorder in the slip plane and as a result a cavity opens in the NW (Fig. 4(b), not visible in the full view of Fig. 3). Afterwards, dislocations are nucleated in secondary {111} planes (red arrows in Fig. 3(b) and red lines in Fig. 4(c)) from the disordered zones of the initially activated slip plane. The opened cavity next extends and starts behaving as a crack tip propagating in the initially activated slip plane (black arrow in Fig. 3(c) and red line in Fig. 4(d)). After extensive deformation, the NW fractures along this slip plane. Fig. 3(d) shows the NW just before fracture, the dotted red circle and the slice view in the inset highlighting the crack.

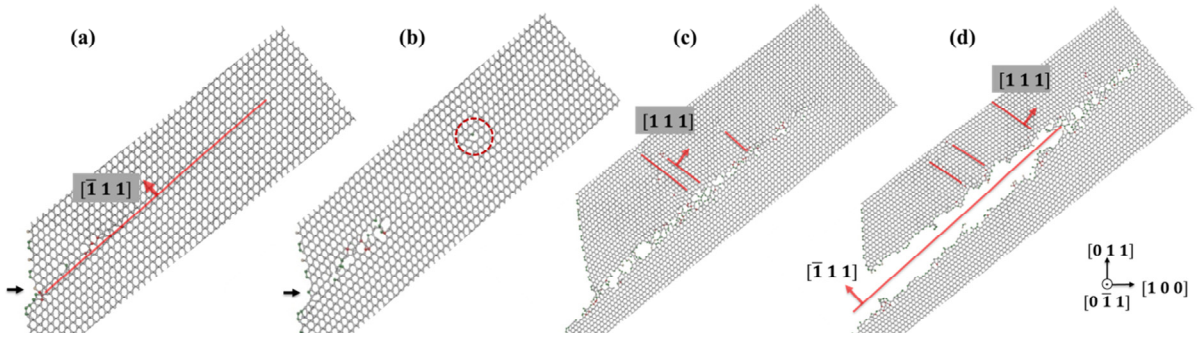


Fig. 4. Slice view of the sequences shown in figure 3. See text for details.

The corresponding elementary mechanisms are indicated with red arrows in the diagram of Fig. 3(e). These include several dislocation nucleations from the surface, formation of disorder through dislocation propagation, dislocation nucleations inside the NW, opening of a cavity, amorphization and final breaking of the NW mainly through cavity extension.

Cavities can also form via dislocation interactions, as shown in Fig. 5 for a test on a smaller NW, with otherwise the same parameters as that of Fig. 3 and 4 (10 K, fresh-cut surface, SW*m* potential). Fig. 5 (a) and (b) show the nucleation and glide of one dislocation from the right surface (core underlined in red and indicated by the red arrow, slip plane indicated with the red line). In Fig. 5(b), the nucleation of another dislocation from the left surface in an adjacent slip plane (black line) is evidenced through the surface step height increase (black arrow). The interaction between these two dislocations (of opposite signs) produces a small cavity (dotted red circle in Fig. 5(c)-(d)). Following multiple dislocations nucleations from the formed cavity, the latter grows inside the NW: in Fig. 5(e) and (f) red and blue arrows and polygons underline two different dislocations nucleated from the cavity, and the black outline in Fig. 5(e)-(g) highlights the resulting expansion of the cavity. The sequences shown in Fig. 5(a)-(g) correspond to the elementary mechanisms indicated by red arrows in Fig. 5(h).

A specific mechanism, which can lead either to cavity opening (not shown here) or to the NW rupture through intensive shear due to dislocations propagation as shown in Fig. 6, is the formation of a "5/7" defect, so called because it is composed of ring pairs of 5 and 7 silicon atoms, as seen in the inset of Fig. 6(b). This defect results from the nucleation and concurrent propagation of two perfect dislocations with different Burgers vectors in the same slip plane, which intersection forms a row of 5/7 atoms rings. Fig. 6(a) shows the nucleation and propagation of one of the two dislocations (slip plane highlighted in red), which emergence at the surface produces the steps indicated with black arrows in Fig. 6(b). In the slice cut view only one of the two dislocations producing the 5/7 defects can be seen. The 5/7 defect is visible inside the red dotted circle in Fig. 6(b). The subsequent nucleation from the zone of the defect and glide of new dislocations in both sets of shuffle slip planes increase the disorder inside the NW (red dotted circle in Fig. 6(c)-(d), where the red lines display some of the slip planes). The NW finally breaks after intensive shear, as indicated in Fig. 6(e) with the elementary mechanisms diagram.

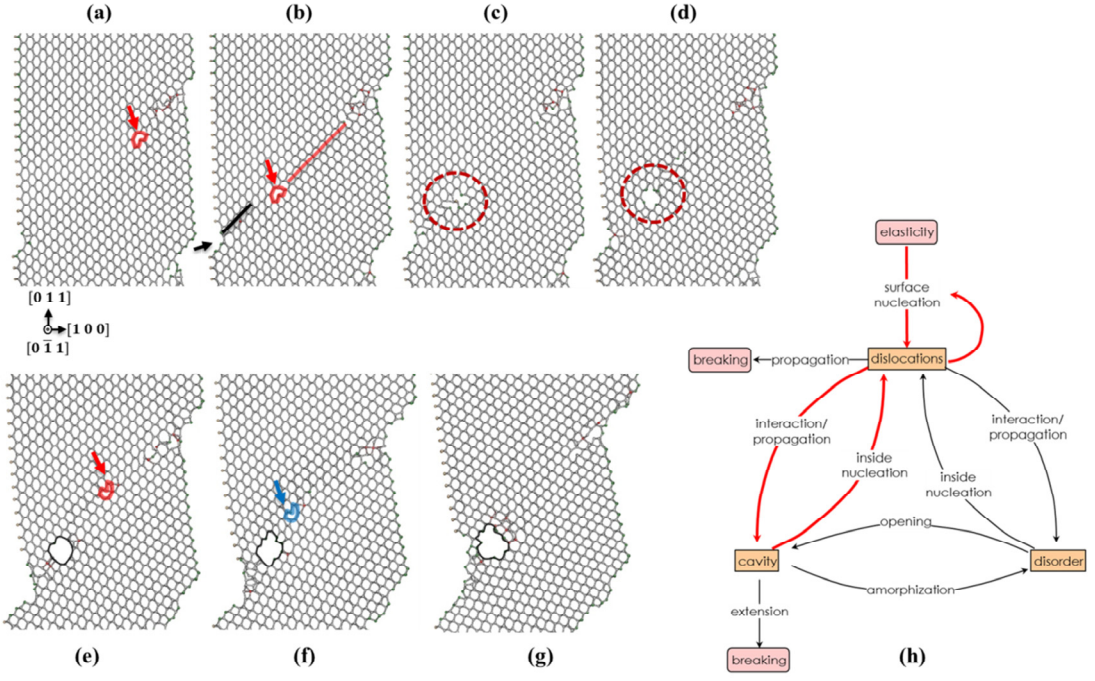


Fig. 5. (a)-(g) Plasticity and cavity opening in a 8 nm diameter NW deformed up to 22% in tension at 10 K (SW*m* potential, $\ell = 21$ nm, fresh-cut surface). See text for details. (h) Corresponding elementary mechanisms (red arrows).

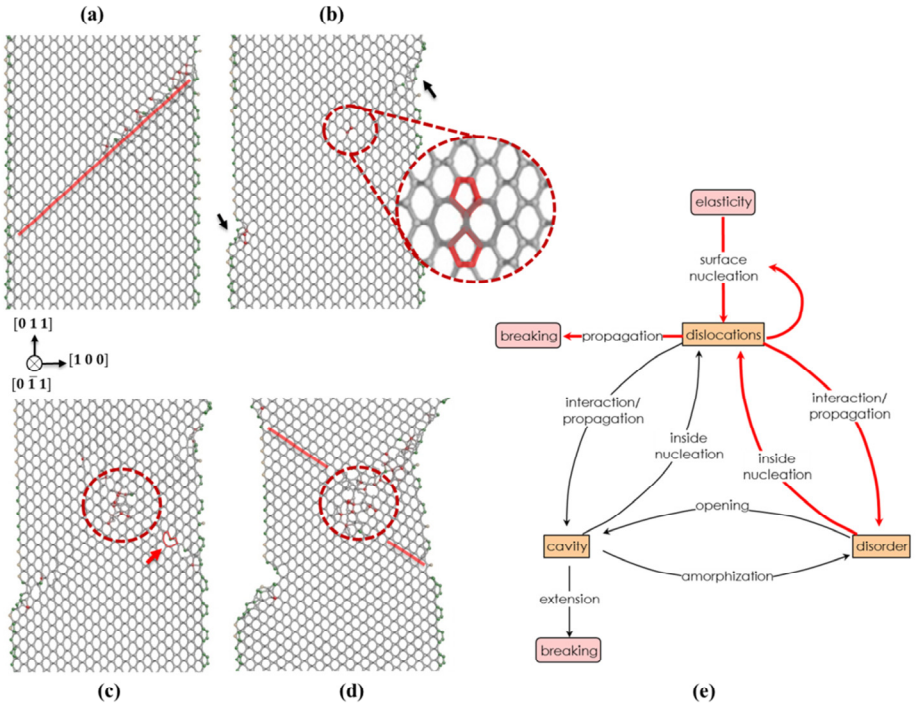


Fig. 6.(a)-(d) Onset of plasticity, 5/7 ring formation and disordering of the atomic structure in a 8 nm diameter NW deformed up to 11% in tension at 10 K (MEAM-G potential, $\ell = 21$ nm, annealed surface). See text for details. (e) Corresponding elementary mechanisms (red arrows).

### *3.3. Comparison with experiments – discussion*

Experimentally, perfect dislocations, disorder and amorphization were observed by high resolution TEM during in situ silicon <110>-NWs deformation in tension at room temperature [10]. The dislocations, supposedly in shuffle set planes, were emitted in the two equivalent {111} planes. In this experimental study, the emission of dislocations induced disordering of the crystalline structure and further amorphization in a fashion similar to some of our simulations (see e.g. Fig. 6(d)), but no crack opening was reported. In another study, perfect dislocations were also observed to form from the tensile region of bent silicon <110>-NWs [12].

To the best of our knowledge, cavity opening and crack propagation are not observed in tensile experiments, either because the NW breaks through cleavage fracture with no such cavity or either because the processes are too fast to be observable (very fast energy release rate as soon as bonds start to break). Crack formation has been observed in silicon pillar compression tests [5,6,19,22]; they are often associated with slip bands, which suggests a dislocation interaction mechanism explaining the formation of those cracks [8]. The mechanism described in [8] has never been detected in our tensile simulations. Some authors of the present paper performed experimental compression tests on smaller pillar (100 nm diameter) and evidenced small cavities which look like those seen in simulations. The description of this experimental study is beyond the scope of this paper and it will be presented in a separate article; nonetheless we show in Fig. 7 typical micrographs of one of the deformed pillar as an example. It exhibits a small cavity (dotted red circle in Fig. 7(b)) in the bottom part of the pillar. Note that it is not a singular case, since similar cavities were detected in several other tests. Because of the large shear in the top part of the pillar, it is possible that local bending arises in the bottom region and consequently that small tensile zones appear. This could explain the formation of this small cavity and its strong resemblance with those observed in tensile simulations (compare e.g. with Fig. 5(d)). Further analyses are in progress on that subject.

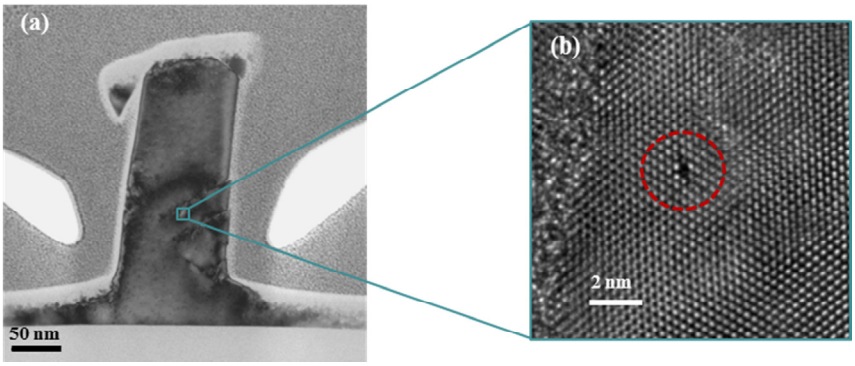


Fig. 7. (a) Bright field TEM micrograph of a 100 nm diameter pillar deformed in displacement controlled mode. (b) High resolution TEM micrograph of the zone framed in (a). The details of the experimental study will be provided in a separate article.

Although the experiments suggest that the behavior of the NWs ensues from different elementary mechanisms, they hardly provide information on their succession or entanglement. In contrast, the detailed description at the atomic level offered by the simulations allows the decomposition and rationalization of the sequences observed. In simulation tests, some of the observed mechanisms are more probable for given conditions (e.g. the "5-7" defects have only been observed at low temperature), others appear in many if not all situations (e.g. surface dislocation nucleation). However, the systematic investigation of the factors controlling the emergence of elementary mechanisms sequences is beyond the scope of this article. Furthermore, because of the great variety of those mechanisms, and their complex entanglement in many cases, it is difficult to obtain a clear panorama of the ductility/brittleness as a function of NW size or temperature. The objective of the ductility parameter presented in the next section is to give a coarse but quantitative assessment of this ductile/brittle behavior for the different situations encountered in simulation tests.

## 4. Towards a quantification of the BDT

### *4.1. Ductility parameter*

In their experimental study of Si NW tensile deformation, Han et al. [10] observed significant plastic deformation for diameters ranging from 15 to 70 nm, and they estimated the BDT diameter via the extrapolation of the curve of the diameter reduction ratio versus diameter. We propose here a ductility parameter based on a similar idea, which is to measure the ratio of the shear produced by dislocations over the initial NW diameter. Since both dislocations and cavities/cracks appear in many of the tensile simulations, the shear produced by dislocations is here evaluated just before cavity formation. If no dislocation is formed before cavity opening, the ductility parameter is zero, characterizing a purely brittle behavior. Conversely, if no cavity opens before the nanowire rupture, the ductility parameter is equal to 1, signature of a purely ductile behavior. Intermediate behaviors such as those described in section 3 will give a value between these two extremes. Note that such ductility parameter is a measure of the ductile/brittle behavior of the studied system under given conditions, and not an intrinsic quantity of the material or of the interatomic potential as is the ductility parameter proposed by Kang and Cai [34].

To detect cavity formation, an automated slicing procedure is applied on a selected set of atomic configurations prior to rupture. The slice thickness is chosen to be slightly greater than the thickness of three atomic planes parallel to the deformation axis, so that cavities can be directly visualized inside the slice. Our proposed ductility parameter is then defined as follows:

$$p_{ductility} = \frac{\Delta R}{d} = \frac{N\, b \cos\alpha}{d} \tag{1}$$

with $\Delta R$ the shear produced by dislocations nucleated before cavity formation, $d$ the nanowire diameter, $N$ the number of dislocations, $b$ the norm of their Burgers vector and $\alpha$ the angle between the Burgers vector and the plane perpendicular to the deformation axis. $\Delta R$ can be estimated from the height of the surface steps produced by dislocations when they emerge at the surface, as indicated in Fig. 1(b). To gain efficiency and to avoid geometrical pitfalls, we used an alternative method, based on the energy variation during a deformation test, to assess the number of dislocations producing shear before cavity opening. Indeed, just before cavity opening, the nanowire is in a state denoted C, with energy $E_c$ and length $\ell_c$ which can be considered to be the sum of the plastic and elastic elongation. So, if the external applied load were removed from this state C, it can be assumed that only the plastic part would remain, and also that the potential energy would return to that of the undeformed system $E_0$. This is an approximation that neglects potential contribution of structural defects, such as surface steps, disorder or dislocation lines remaining in the NW after relaxation. The nanowire would thus be in a state called P, with length $\ell_0 + N\,b\,\sin\alpha$ (undeformed length plus elongation due to plasticity). Note that except for checking purpose, it is not necessary to really perform this relaxation. If we assume that the energy variation between states P and C is purely elastic with the same Young modulus $E$ than for a pristine NW, it can be written:

$$E_c - E_0 = \frac{1}{2} V\, E\, \varepsilon^2 = \frac{1}{2} V\, E \left[ \frac{\ell_c - (\ell_0 + N\,b\sin\alpha)}{(\ell_0 + N\,b\sin\alpha)} \right]^2 \tag{2}$$

$V$ being the nanowire volume (supposed to be constant during deformation, which is partly justified by the Poisson effect) and $\varepsilon$ the elastic deformation between states P and C. The number $N$ of dislocations producing shear is then easily extracted from equation (2). We tested the assumptions made for a few tests, on the one hand by removing the external applied load and relaxing the system potential energy, and on the other hand by counting directly the number of dislocations before cavity opening. We then observed that equation (2) underestimates the ductility parameter but that it still gives the correct trends, so that it can be used to analyze the role of the different simulation conditions. It must be stressed that all methods (equation (2) and direct counting) take into account all shears, even if different sources of shear are activated.

Our proposed ductility parameter explicitly depends on the NW diameter, to reflect the higher impact of a given shear in a smaller NW. It is also intrinsically affected by the system size. Indeed, for larger NW, dislocations travelling distances are larger, so that the probability of dislocation interactions, and then that of cavity/crack opening is higher. Since the ductility parameter is calculated just before cavity opening, the impact of dislocations travelling distances is naturally incorporated in it.

### *4.2. Discussion*

The ductility parameters determined from equations (1) and (2) for various simulations are displayed in table 1.

Table 1. Ductility parameter for tests performed under various conditions.

| test | i | ii | iii | iv | v | vi | vii | viii | ix | x | xi |
|---|---|---|---|---|---|---|---|---|---|---|---|
| potential | ←— | | SW*m* | | | —→ | ← | | MEAM-G | | → |
| NW diameter $d$ (nm) | 8 | 8 | 45 | 45 | 45 | 45 | 8 | 8 | 8 | 44 | 44 |
| NW length $\ell$ (nm) | 8 | 75 | 46 | 75 | 46 | 46 | 31 | 31 | 31 | 38 | 38 |
| ratio $\ell$/d | 1.0 | 9.4 | 1.0 | 1.7 | 1.0 | 1.0 | 3.9 | 3.9 | 3.9 | 0.9 | 0.9 |
| temperature $T$ (K) | 10 | 10 | 10 | 10 | 300 | 600 | 10 | 10 | 10 | 10 | 10 |
| $p_{ductility}$ | 0.78 | 0.34 | 0.06 | 0.04 | 0.05 | 0.10 | 0.26 | 0.10 | 0.06 | 0.01 | 0.01 |

First of all, it should be emphasized that the ductility parameter was calculated for a limited number of tests, so that the discussion below provides trends that would need to be confirmed by a statistical study. Let's first compare the values obtained with MEAM-G potential for tests vii, viii and ix, performed under the same conditions (only the

initial distributions of atomic velocities were changed): the ductility parameter varies from 0.06 to 0.26, giving an idea of its scattering. Such a scattering seems to be reduced for larger NWs, as seen for tests x and xi also performed under the same conditions. This can be understood because a same variation of the global shear has less effect in a large NW than in a smaller one. Next, we notice that different values are obtained with both potentials for NWs of similar sizes at the same temperature (compare e.g. test iii and tests x or xi). This is not surprising given the strong interatomic potential dependency of fracture and plasticity properties for covalent materials such as silicon. The ductility parameter reflects the known tendencies of the interatomic potentials: it is higher for SW*m* which favors plasticity compared to MEAM-G. Nonetheless, the values of the ductility parameter are of the same order for tests performed under similar conditions. Besides, they exhibit the same trend when the NW diameter increases, that is a decrease. Such a decrease is noteworthy for SW*m* potential: for example from 0.34 for $d = 8$ nm (test ii) to 0.04 for $d = 45$ nm (test iv), all others parameters being equal. The decrease of the ductility parameter when the NW diameter increases is less important, though still significant for MEAM-G potential (compare tests vii, viii or ix with tests x or xi). Finally, the effect of the NW length and the influence of the temperature were examined with SW*m* potential only. At low temperature, the ductility parameter decreases when the NW length increases (compare tests i and ii, or tests iii and iv), in agreement with our previous study [32]. The length effect at higher temperatures still needs to be investigated. When the temperature increases, the ductility parameter seems overall to increase (cf. tests iii-v and vi). Though the increase of ductility with temperature and its decrease with NWs size could have been expected, it is worth noting that the ductility parameter allows a quantitative assessment of these behaviors. Moreover, its scattering among the different tests performed indicates that in NWs the BDT may not be abrupt, in particular with temperature, unlike what is observed in bulk silicon.

## 5. Conclusion

The NW tensile simulations performed show a great variety of mechanisms at the atomic scale. The NW behavior results from a more or less complex sequence of these elementary mechanisms, which can be described with a diagram linking the structural defects observed. Such structural defects – perfect dislocations, disordered zones and cavities – are also observed experimentally in deformed NWs or nanopillars.

Only perfect dislocations in shuffle set planes are observed in the simulations presented in this article. Previous MD simulations in a different configuration [18] indicate a change from perfect shuffle dislocations to partial glide dislocations for temperatures above 900K (this value is higher than that obtained in experiments, which can be explained by the very small time scales inherent to MD simulations). Thus, it can not be ruled out that partial glide dislocations would form in the specific configuration studied here, and the results described here are then fully relevant for low to moderate temperatures.

For such temperatures, the simulations greatly help understanding the links between the structural defects; they evidence for example the cavity opening resulting from dislocation interactions. Indeed, nano-objects are characterized by the absence of pre-existing cracks so that cavity/crack formation is a preliminary step for brittleness. The simulations also reveal that dislocation nucleation and cavity opening, as well as dislocation propagation and cavity extension, often coexist, which makes delicate to discriminate between ductile and brittle behavior in many cases.

The introduced ductility parameter allows a quantitative analysis of the observed trends: increase of the ductility with temperature, and decrease with NW size (diameter or length). It underlines the non-abrupt character of the BDT for NWs: the ductility parameter does not go sharply from 0 to 1 when the diameter decreases or when the temperature increases. This smooth character of the BDT with temperature is in contrast with what is observed in bulk silicon. A thorough study of the ductility parameter scattering (with e.g. a statistical survey) would give useful information on the BDT in nano-objects.

## Acknowledgements

We wish to thank “l’Agence Nationale de la Recherche” for the financial support for this research under the grant reference ANR-12-BS04-0003-01.

This work pertains to the French Government program “Investissements d’Avenir” (LABEX INTERACTIFS, reference ANR-11-LABX-0017-01).

Computations have been performed on the supercomputer facilities of the Mésocentre de calcul Poitou-Charentes.

## References

[1] T. Zhu, J. Li, Progress in Materials Science 55 (2010) 710-757.

[2] J.R. Greer, J.Th.M. de Hosson, Progress in Materials Science 56 (2011) 654-724.

[3] G. Stan, S. Krylyuk, A.V. Davydov, I. Levin, R.F. Cook, Nano Letters 12 (2012) 2599-2604.

[4] S. Hoffmann, I. Utke, B. Moser, J. Michler, S.H. Christiansen, V. Schmidt, S. Senz, P. Werner, U. Gŏsele, C. Ballif, Nano Letters 6 (2006) 622-625.

[5] F. Ostlund, K. Rzepiejewska-Malyska, K. Leifer, L.M. Hale, Y. Tang, R. Ballarini, W.W. Gerberich, J. Michler, Advanced Functional Materials 19 (2009) 2439-2444.

[6] J. Rabier, A. Montagne, J.M. Wheeler, J.L. Demenet, J. Michler, R. Ghisleni, Phys.Status Solidi C 10 (2013) 11-15.

[7] J. Michler, K. Wasmer, S. Meier, F. Ostlund, Applied Physics Letters 90 (2007) 043123.

[8] F. Ostlund, P.R. Howie, R. Ghisleni, S. Korte, K. Leifer, W. Clegg, J. Michler, Phil. Mag. 91 (2011) 1190-1199.

[9] L. Thilly, R. Ghisleni, C. Swistak, J. Michler, Phil. Mag. 92 (2012) 3315-3325.

[10] X. Han, K. Zheng, Y.F. Zhang, X. Zhang, Z. Zhang, Z.L. Wang, Advanced Materials 19 (2007) 2112-2118.

[11] D.M. Tang, C.L. Ren, M.S. Wang, X. Wei, N. Kawamoto, C. Liu, Y. Bando, M. Mitome, N. Fukata, D. Golberg, Nano Letters 12 (2012) 1898-1904.

[12] K. Zheng, X. Han, L. Wang, Y. Zhang, Y. Yue, Y. Qin, X. Zhang, Z. Zhang, Nano Letters 9 (2009) 2471-2476.

[13] C. St. John, Phil. Mag. 32 (1975) 1193-1217.

[14] J. Samuels, S.G. Roberts, Proc. R. Soc. Lond. A 421 (1989) 1-23.

[15] P.D. Warren, Scripta Metallurgica 23 (1989) 637-642.

[16] D. Sen, C. Thaulow, S.V. Schieffer, A. Cohen, M.J. Buehler, Phys. Rev. Lett. 104 (2010) 235502.

[17] J. Rabier, J.L. Demenet, Scripta Materialia 45 (2001) 1259-1265.

[18] J. Godet, P. Hirel, S. Brochard, L. Pizzagalli, Phys.Status Solidi A 206 (2009) 1885-1891.

[19] S. Korte, J.S. Barnard, R.J. Stearn, W.J. Clegg, International Journal of Plasticity 27 (2011) 1853-1866.

[20] W. Kang, M.T.A. Saif, Advanced Functional Materials 23 (2013) 713-719.

[21] Y. Zhu, F. Xu, Q. Qin, W.Y. Fung, W. Lu, Nano Letters 9 (2009) 3934-3939.

[22] Y.C. Wang, D.G. Xie, X.H. Ning, Z.W. Shan, Applied Physics Letters 106 (2015) 081905.

[23] Y. Bolkhovityanov, A.S. Deryabin, A.K. Gutakovskii, M.A. Revenko, L.V. Sokolov, Applied Physics Letters 85 (2004) 6140-6142.

[24] B. Pichaud, N. Burle, M. Texier, C. Alfonso, M. Gailhanou, J. Thibaoult-Pénisson, C. Fontaine, V.I. Vdovin, Phys.Status Solidi C 6 (2009) 1827-1835.

[25] S. Brochard, P. Beauchamp, J. Grilhé, Phil. Mag. A 80 (2000) 503-524.

[26] J. Godet, L. Pizzagalli, S. Brochard, P. Beauchamp, Phys. Rev. B 70 (2004) 054109.

[27] J. Godet, S. Brochard, L. Pizzagalli, P. Beauchamp, J.M. Soler, Phys. Rev. B 73 (2006) 092105.

[28] P. Hirel, S. Brochard, L. Pizzagalli, P. Beauchamp, Scripta Materialia 57 (2007) 1141-1144.

[29] Y. Liu, E. Van der Giessen, A. Needleman, International Journal of Solids and Structures 44 (2007) 1719-1732.

[30] K. Kang, W. Cai, International Journal of Plasticity 26 (2010) 1387-1401.

[31] Q. Liu, S. Shen, International Journal of Plasticity 38 (2012) 146-158.

[32] F. Abed El Nabi, J. Godet, S. Brochard, L. Pizzagalli, Modelling Simul. Mater. Sci. Eng. 23 (2015) 025010.

[33] J. Godet, F. Abed El Nabi, S. Brochard, L. Pizzagalli, Phys.Status Solidi A 212 (2015) 1643-1648.

[34] K. Kang, W. Cai, Phil. Mag. 87 (2007) 2169-2189.

[35] S. Plimpton, J. Comp. Phys. 117 (1995) 1-19.

[36] L. Verlet, Phys. Rev. 159 (1967) 98-103.

[37] W.G. Hoover, Phys. Rev. A 31 (1985) 1695-1697.

[38] F.H. Stillinger, T.A. Weber, Phys.Rev. B 31 (1985) 5262-5271.

[39] L. Pizzagalli, J. Godet, J. Guénolé, S. Brochard, E. Holmstrom, K. Nordlund, T. Albaret, J. Phys.: Condens. Matter 25 (2013) 055801.

[40] J. Godet, L. Pizzagalli, S. Brochard, P. Beauchamp, J. Phys.: Condens. Matter. 15 (2003) 6943-6953.

[41] M.I. Baskes, Phys. Rev. B 46 (1992) 2727-2742.

[42] J. Godet, C. Furgeaud, L. Pizzagalli, M.J. Demkowicz, Extreme Mechanics Letters 8 (2016) 151-159.

[43] J. Guénolé, J. Godet, S. Brochard, Modelling. Simul. Mater. Sci. Eng. 19 (2011) 074003.

[44] T. Zhu, J. Li, A. Samanta, A. Meach, K. Gall, Phys. Rev. Lett. 100 (2008) 025502.

[45] J. Li, Modelling. Simul. Mater. Sci. Eng. 11 (2003) 173-177.